Journal of Molecular and Cellular Cardiology 191 (2024) 40–49

Contents lists available at ScienceDirect

Journal of Molecular and Cellular Cardiology

journal homepage: www.elsevier.com/locate/yjmcc

# Titin's cardiac-specific N2B element is critical to mechanotransduction during volume overload of the heart

Joshua Strom [a,d,1], Mathew Bull [a,d,1], Jochen Gohlke [a,d], Chandra Saripalli [a,d], Mei Methawasin [a,d], Michael Gotthardt [b,c], Henk Granzier [a,*]

[a] Department of Cellular and Molecular Medicine, University of Arizona, Tucson, AZ 85721, United States of America
[b] Max Delbrück Center for Molecular Medicine in the Helmholtz Association, Berlin, Germany
[c] Department of Cardiology, Charité-Universitätsmedizin Berlin, Berlin, Germany
[d] Sarver Molecular Cardiovascular Research Program, University of Arizona, Tucson, AZ 85721, United States of America

ARTICLE INFO

*Keywords:*
Titin
Mechanosensing
Pressure/volume overload
Hypertrophy

ABSTRACT

The heart has the ability to detect and respond to changes in mechanical load through a process called mechanotransduction. In this study, we focused on investigating the role of the cardiac-specific N2B element within the spring region of titin, which has been proposed to function as a mechanosensor. To assess its significance, we conducted experiments using N2B knockout (KO) mice and wildtype (WT) mice, subjecting them to three different conditions: 1) cardiac pressure overload induced by transverse aortic constriction (TAC), 2) volume overload caused by aortocaval fistula (ACF), and 3) exercise-induced hypertrophy through swimming. Under conditions of pressure overload (TAC), both genotypes exhibited similar hypertrophic responses. In contrast, WT mice displayed robust left ventricular hypertrophy after one week of volume overload (ACF), while the KO mice failed to undergo hypertrophy and experienced a high mortality rate. Similarly, swim exercise-induced hypertrophy was significantly reduced in the KO mice. RNA-Seq analysis revealed an abnormal β-adrenergic response to volume overload in the KO mice, as well as a diminished response to isoproterenol-induced hypertrophy. Because it is known that the N2B element interacts with the four-and-a-half LIM domains 1 and 2 (FHL1 and FHL2) proteins, both of which have been associated with mechanotransduction, we evaluated these proteins. Interestingly, while volume-overload resulted in FHL1 protein expression levels that were comparable between KO and WT mice, FHL2 protein levels were reduced by over 90% in the KO mice compared to WT. This suggests that in response to volume overload, FHL2 might act as a signaling mediator between the N2B element and downstream signaling pathways. Overall, our study highlights the importance of the N2B element in mechanosensing during volume overload, both in physiological and pathological settings.

## 1. Introduction

The heart possesses remarkable adaptability to both physiological and pathological stressors, employing hypertrophy as a vital long-term adaptation mechanism [1]. Aside from genetic and environmental factors, the heart encounters two main types of hemodynamic stress: altered preload and altered afterload. While the impact of neurohormonal signaling on cardiac hypertrophy is well-established, recent attention has focused on identifying cellular sensors capable of directly perceiving mechanical load changes and transmitting them as downstream signaling events [2].

Several potential mechanosensors have been identified within the sarcolemma and cytoskeletal network, including the sarcomere [3]. Within the sarcomere, titin is well positioned to play a role in sensing mechanical alterations during systole and diastole. Spanning from the *Z*-disk to the M-band, titin interacts directly with both thin and thick filaments of the sarcomere [4]. It serves as the primary regulator of passive stiffness in the sarcomere and acts as a binding site for various proteins involved in transmitting biomechanical signals [5,6]. The N2B spring element, located in the elastic I-band region of titin, is specifically expressed in cardiac myocytes (Supplemental Fig. 1 A). Comprising a 572 amino acid sequence flanked by tandem Ig segments, the N2B

* Corresponding author at: Medical Research Building (MRB), Room 325. 1656 E Mabel Street, Tucson, AZ 85724-5217, United States of America.
*E-mail address:* granzier@arizona.edu (H. Granzier).
[1] These authors contributed equally.

https://doi.org/10.1016/j.yjmcc.2024.04.006
Received 26 July 2023; Received in revised form 9 March 2024; Accepted 8 April 2024
Available online 10 April 2024

element is predicted to possess coiled-coil α-helical conformations [7,8]. Detailed investigation of titin's extensibility in cardiac tissue has revealed that the N2B element undergoes extension during diastole, particularly when the end-diastolic volumes are near the upper end of their physiological range [9,10]. The N2B element hosts various signaling proteins, including the scaffolding proteins FHL1 and FHL2 (four-and-a half LIM domains 1 and 2) [11]. Moreover, the N2B element itself serves as a substrate for nodal kinases implicated in heart disease, such as PKA [12], PKG [13], CAMKIIδ [14–16], and ERK2 [17]. Due to its strategic location in the sarcomere, elastic properties, and interactions with relevant signaling pathways, the N2B element has been proposed to function as a mechanosensor, converting changes in titin strain into biochemical signals [18].

In this study, we aimed to investigate the role of titin's cardiac-specific N2B element as a sensor for stress-induced remodeling of the heart. To achieve this, we utilized a previously published murine model where the N2B element has been excised (Supplemental Fig. 1 A), referred to as N2B KO [19]. We subjected the mice to hemodynamic stress by increasing afterload (TAC surgery) or preload (ACF surgery). Additionally, we examined the role of the N2B element in physiological hypertrophy induced by endurance exercise training (swimming). Our findings revealed that the N2B element is necessary for the hypertrophy response to increased preload but dispensable for afterload-induced hypertrophy. RNA-Seq analysis indicated an impaired β-adrenergic response in N2B KO mice following ACF, consistent with the blunted response to isoproterenol-induced hypertrophy observed in these mice. Western blot analysis of canonical hypertrophy signaling kinases demonstrated attenuated activation of p38 MAPK in N2B KO mice one week after ACF. Furthermore, FHL2 protein levels were reduced by over 90% in N2B KO mice compared to wild-type mice. Considering FHL2's involvement in modulating the hypertrophic response [20–22], it is a potential mediator of signaling events between the N2B element and downstream signaling pathways in the setting of volume overload.

## 2. Methods

### 2.1. Mice

N2B KO mice were used that had the N2B element (exon 49) removed and only homozygous mice were used [23]. Wild type littermate mice functioned as controls. All mice were on a C57BL/6 J background, male, and were studied at 4 months of age. In the N2B KO the deletion of exon 49 removes 2646 bp (882 aa) and maintains the open reading frame. To evaluate the possibility that deleting the N2B element caused aberrant splicing of spring element exons, the PSI (percent spliced in) of all exons was determined using RNAseq. This confirmed that exon 49 is absent with no major changes in PSI elsewhere in titin's spring region (Supplemental Fig. 1B). For the isoproterenol study, mice were injected with isoproterenol (2 mg/kg/day; subcutaneously) or an equivalent volume of saline daily for 5 consecutive days. All experiments were approved by the University of Arizona Institutional Animal Care and Use Committee and followed the U.S. National Institutes of Health Using Animals in Intramural Research guidelines for animal use.

### 2.2. TAC surgery

Male mice were subjected to minimally invasive transverse aortic constriction (TAC) as previously described [24]. Briefly, mice were anesthetized using a single injection of ketamine and xylazine (120 mg/kg and 12 mg/kg, I.P.) and a 5 mm horizontal incision was made at the first left intercostal space. The thymus was temporarily retracted to visualize the aortic arch and a 7–0 silk suture was passed under the aorta between the right innominate and left carotid arteries. The suture was ligated around a blunted 27-gauge needle and the needle was quickly removed. The chest wall and skin were closed. Mice were euthanized 1 week following surgery.

### 2.3. ACF surgery

Aortocaval fistula (ACF) surgeries were performed in mice to evaluate the cardiac response to volume overload as previously described [16]. Briefly, a midline abdominal incision was made, and blunt dissection exposed the abdominal aorta and inferior vena cava (IVC). Vascular clips were placed above the iliac bifurcation and below the iliolumbar vessels. A 23-g needle was inserted into the aorta and through the common mid-wall of the IVC, creating an ACF. The needle was removed, and cyanoacrylate glue (Vetbond) was used to seal the aortic puncture. Shunt patency was visually confirmed by mixture of bright red arterial blood in the IVC. Mice were euthanized 1- or 4-weeks following surgery. The 4-week time point was selected after it became clear that ~40% of the N2BKO mice died within the first week after ACF surgery.

### 2.4. Swimming study

A swimming chamber for mice was developed to control duration and pace of swimming. A magnetically driven water circulator was attached to the side of the tank to produce a current across the tank, which the mice swam against. Mice swam for 1 h twice a day for three weeks after an initial ramp up phase. The swimming chamber temperature was held constant at 29 °C.

All experiments were approved by the University of Arizona Institutional Animal Care and Use Committee and followed the U.S. National Institutes of Health *Using Animals in Intramural Research guidelines for animal use*.

### 2.5. Protein expression analysis

Flash frozen LV tissues were pulverized in liquid nitrogen and then solubilized in urea buffer (in mol/L: 8 urea, 2 thiourea, 0.05 tris-HCl, 0.075 dithiothreitol with 3% SDS and 0.03% bromophenol blue, pH 6.8) and 50% glycerol with protease inhibitors (in mmol/L: 0.04 E64, 0.16 leupeptin and 0.2 PMSF) at 60 °C for 10 min. Samples were centrifuged at 13,000 RPM for 5 min, aliquoted, flash frozen in liquid nitrogen, and stored at −80 °C. For Western blotting, solubilized samples were run using an SDS-PAGE, then transferred onto polyvinylidene difluoride membranes using a semi-dry transfer unit (Trans-Blot Cell, Bio-Rad). Blots were stained with Ponceau S to visualize the total protein transferred. Blots were then probed with primary antibodies followed by secondary antibodies conjugated with infrared fluorescent dyes. Blots were scanned using an Odyssey Infrared Imaging System (Li-COR Biosciences).

### 2.6. Myocyte cross section area

OCT (Tissue-Tek) embedded hearts were sectioned in 7 μm thick cross sections and stored at −20 °C overnight. The cross-sections were permeabilized with 1% triton X-100 and stained with α-actinin (vendor) for myocyte identification and anti-Laminin (vendor) to demarcate cell borders. Images were collected on an Axio Imager M.1 microscope (Carl Zeiss) using an Axio Cam MRC (Carl Zeiss). CSAs were measured using the ImageJ program (National Institutes of Health) and their borders of stained cells that included nuclei were traced manually. The CSA of 100 myocytes from the myocardium of the left ventricle were collected from each sample ($n = 3$ mice per group).

### 2.7. RNA Sequencing (RNA-Seq)

LV tissue from 1-week ACF hearts were collected and stored in RNA later in order to preserve RNA integrity. We studied tissues from 8 mice for each group and pooled two LV tissues providing four samples per group for RNAseq to reduce biological variance while keeping sample sizes manageable. For RNA extraction, 600 μl pre-chilled buffer RLT (RNeasy Fibrous Tissue Mini Kit, Qiagen) with 1% β-Mercaptoethanol

was added to muscle tissue stored in RNAlater in a 4 ml cryovial. Tissue was disrupted using a rotor-stator-homogenizer for 30 s. A protein digest was performed by adding 600 µl RNase-free water containing 6 mAU Proteinase K and incubating at 55 °C for 10 min. Samples were transferred to a 1.5 ml microfuge tube and centrifuged for 3 min at 14000 *g*. The supernatant was transferred to a 2 ml tube with 600 µl Ethanol and transferred to an RNeasy mini spin column. Thereafter, RNA extraction was performed following the manufacturer's instructions and quantified using a Nanodrop ND-1000 spectrophotometer (Thermo Scientific).

For the library preparation, rRNA was depleted from RNA preparations with a NEBnext rRNA depletion kit using 1 µg total RNA as starting material. Libraries were prepared using the NEBNext Ultra II Directional RNA Library Prep Kit for Illumina following the manufacturer's instructions. RNA was fragmented for 10 min at 94 °C. For first strand cDNA synthesis, incubations were performed for 10 min at 25 °C followed by 50 min at 42 °C and 15 min at 70 °C. For size selection, conditions for an approximate insert size of 300 bp were used. Size-selected libraries were enriched by PCR for 10 cycles and purified using NEBnext sample purification beads. Library quality was checked using a fragment analyzer and sequencing performed on an Illumina Hiseq2500 sequencer using 100 bp paired-end sequencing.

Adapters and low-quality reads were removed with Trim Galore (http://www.bioinformatics.babraham.ac.uk/projects/trim_galore/) and reads were mapped to the mouse genome (Release M17 GRCm38.p6) using STAR with default settings. Differentially expressed genes were determined with DESeq2. Genes with adjusted *p*-values lower than 0.05 were considered to be differentially expressed. Selected differentially expressed genes were analyzed in *N2B KO* samples using Western blots to check if changes in gene expression correlate with altered protein levels.

For calculating the inclusion percentage of all exons from titin transcripts, inclusion reads and exclusion reads were counted for each exon based on annotation from Bang et al. for titin [25]. Inclusion reads (IR) are reads overlapping the exon being investigated, normalized by exon length. Exclusion reads (ER) are reads either upstream or downstream that support exclusions of the read. From these factors the following equations were used to calculate the percent spliced in index (PSI) as a measure of much an exon is spliced in:

$$IR_{i,n} = \frac{IR_i}{length\ exon_i + read\ length - 1}$$

$$ER_{i,n} = \frac{ER_i}{read\ length - 1}$$

$$PSI_i = \frac{IR_{i,n}}{IR_{i,n} + ER_{i,n}}\%$$

Where $i$ is the exon number and $n$ is the normalized read counts. Determination of differential exon usage was performed after adjusting exon counts to gene counts by:

$$E^A_{ijk} = \frac{E_{ijk} \times \overline{G}_j}{G_{jk}}$$

Where $E^A_{ijk}$ is the adjusted exon count for exon $i$ of gene $j$ in sample k, $E_{ijk}$ is the raw exon count for exon $i$ of gene $j$ in sample $k$. $\overline{G}_j$ is the mean raw count for gene $j$ for all samples and $G_{jk}$ is the raw gene count for gene $j$ in sample $k$. Adjusted exon counts were then used as input for a statistical analysis identical to the method provided for analysis of differential gene expression provided by the edgeR package.

### 2.8. Calcineurin assay

Calcineurin activity was assayed using LV tissue from mice following 1-week ACF according to the manufacturer's directions (Enzo Life Sciences, New York, USA). Briefly, LV tissue was homogenized in lysis buffer and centrifuged at 16,000 x*g* (4 °C, 30 min). The Supernatant was collected and desalted by column filtration. Calcineurin activity was calculated by subtracting phosphatase activity in the presence of EGTA from total phosphatase activity.

### 2.9. Statistics

Statistical analysis was performed in GraphPad Prism vs 9.3 (GraphPad Software, Inc). Group significance was defined using one or two-way ANOVA followed by multiple testing correction. The student *t*-test was used when comparing two groups and Log-Rank Mantel-Cox test was used to analyze survival. Results are shown as mean ± standard deviation of the mean, $p < 0.05$ was considered significant.

## 3. Results

### 3.1. The N2B element is dispensable for pressure overload-induced hypertrophy

In order to examine whether the N2B element serves as the biomechanical sensor involved in pressure-overload induced hypertrophy, we conducted a study involving N2B knockout (KO) and wild-type (WT) mice that underwent transverse aortic constriction (TAC). The N2B KO and WT mice had comparable survival rates following TAC surgery (Fig. 1A). Additionally, significant left ventricular hypertrophy was observed in both WT and KO mice, as shown in Fig. 1B and Table 1. When normalized to the sham group, the degree of hypertrophy in the KO mice was similar to that of the WT controls (Fig. 1C). To assess the pressure gradient across the trans-stenotic region, echocardiography was performed one week after TAC, and a linear regression analysis was conducted to examine the relationship between pressure and hypertrophy. The results indicated that WT and KO mice exhibited similar responses across the range of pressures studied (Fig. 1D). We also measured the cross-sectional area (CSA) of left ventricular myocytes following TAC, which revealed a robust and comparable increase in CSA in WT and KO mice (Fig. 1E and F), consistent with the tissue weight results. Hence, in response to pressure overload, N2B KO mice exhibit hypertrophy similar to WT mice, indicating that the N2B element is not essential for pressure-induced hypertrophy.

Previously, FHL1 was suggested to play a central role in TAC-induced hypertrophy by binding to the N2B element and acting as a scaffold for a MAPK complex, which transduces stretch signals into hypertrophy signaling [26]. Thus, we measured the expression levels of FHL1 protein in the left ventricle following TAC. The results demonstrated a significant elevation of FHL1 protein in response to TAC; however, no genotype effect was observed (Supplemental Fig. 2). This suggests that FHL1 operates independently of the N2B element to mediate the hypertrophic response.

### 3.2. Volume overload-induced hypertrophy is attenuated in N2B KO mice

While the N2B element is not essential for pressure-induced hypertrophy, its location within the extensible I-band region of titin makes it well-suited to sense biomechanical changes associated with sarcomere stretch, such as those occurring increased preload. To investigate the potential role of the N2B element in responding to preload changes, we conducted two experiments: one group of mice underwent aortocaval fistula (ACF) surgery to induce pathological volume overload, and another group underwent swim exercise to induce physiological volume overload. ACF surgery involved creating a shunt between the abdominal aorta and inferior vena cava (IVC), increasing volume return to the heart and causing volume overload. This leads to an increase in preload and an increase in contractility, and over time this leads to cardiac hypertrophy. The ACF-induced volume overload model has been used previously in dogs, rats and mice [16,27–29]. The patency of the fistula was confirmed through Doppler imaging of the IVC one-week post-surgery

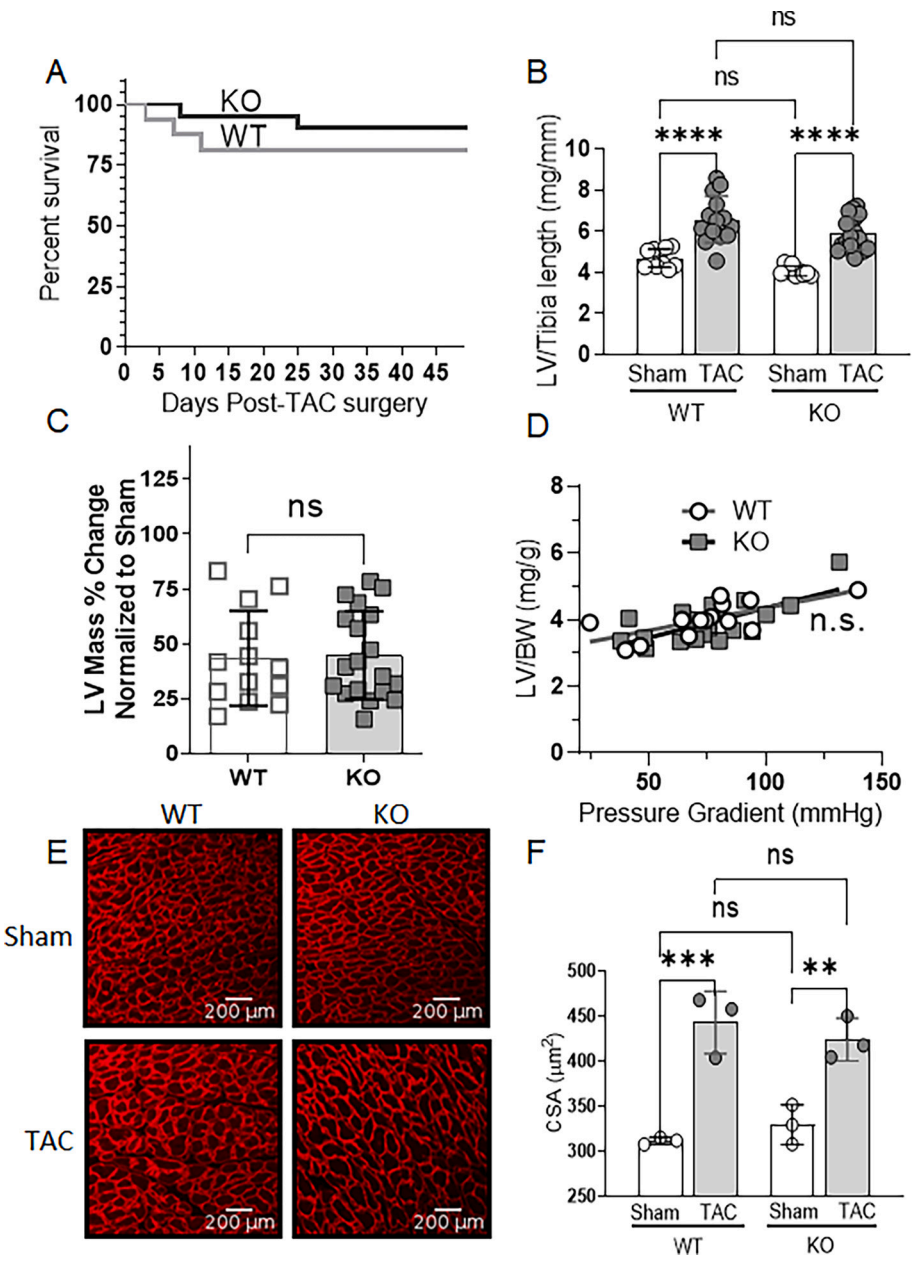


**Fig. 1.** Preserved hypertrophic response to pressure-overload in N2B KO mice. A) Survival curve post TAC surgery, reveals that KO mice tolerate pressure overload equally well as WT mice. B) Left ventricular mass (LV) normalized to tibia length. Two-way ANOVA reveals a significant effect of TAC on LV mass ($p < 0.0001$) and a significant effect of genotype ($p = 0.005$) with KO animals having lower mean values. Results of post-hoc analyses shown on the fig. C) Percent left ventricle (LV) mass increase in TAC relative to sham. The LV mass increase in response to TAC is the same in WT and KO animal ($p = 0.86$). D) LV hypertrophy versus pressure gradient shows no difference between WT and N2B KO mice. E) Laminin-stained LV cross sections. F) cross-sectional area (CSA) measurements. Two-way ANOVA reveals a significant effect of TAC on CSA, but there is no genotype effect. Data shown as mean ± SD (each data point is the average of 300 cells from one mouse). Additional statistical details are in Supplemental Table 3. **:$p < 0.01$; ***:$p < 0.001$; ****:$p < 0.0001$.

(data shown in Supplemental Fig. 3). No mortality was observed in WT mice throughout the entire one-month period following ACF surgery. In contrast, the N2B KO mice exhibited survival for the first three days, followed by a substantial die-off (~40% mortality) over approximately four days, after which lethality was limited (Fig. 2A). Surviving N2B KO and WT mice were examined one week after ACF surgery. We observed significant hypertrophic remodeling in the left ventricle of WT mice, while N2B KO mice showed no effect (Fig. 2B). Compared to sham controls, WT mice exhibited a 26.6 ± 3.3% increase in LV mass (mean ± SD, $n = 9$), whereas KO mice failed to initiate a hypertrophic response, with a change in LV mass of −1.2 ± 0.3% (mean ± SD, n = 9) (Fig. 2B). Continued volume overload for four weeks led to sustained LV hypertrophy in WT mice, with an observed increase in LV mass of 63 ± 18% (mean ± SD, $n = 10$) (Fig. 2C). During this time, KO mice were able to initiate a hypertrophic response of 40 ± 15% (mean ± SD, n = 9), but the extent of hypertrophy was significantly reduced compared to WT controls (Fig. 2C). We also performed an echo analysis on mice that underwent the volume overload surgery (see Supplemental fig. 4 A-G). The results show that in response to volume overload, the LV dimensions are increased in both genotypes (Supplemental Fig. 4E). However, LV wall thickness was significantly increased in the WT but not in KO mice (Supplemental Fig. 4F), a finding consistent with the reduced LV hypertrophy of the KO mice (Fig. 2C). The increase in wall thickness in WT mice will lower wall stress (according to the La Place law) and

**Table 1**
Tissue weights of mice subjected to TAC (left), ACF (middle-left), swimming (middle-right), or isoproterenol (right). BW, indicates body weight; HW, heart weight, LV, left ventricle; RV, right ventricle;LA, left atria; RA, right atria. Statistical significance calculated with two-way ANOVA with Sidak's multiple testing correction. Data shown as mean ± SD. Treatment comparison (TAC vs SHAM; ACF vs SHAM, swimming vs sedentary, and Iso vs saline) indicated by asterisks. Genotype comparison indicated by hashtags. (single symbols $p < 0.05$; double symbols $p < 0.01$; triple symbols $p < 0.001$; quadruple symbols $p < 0.0001$).

| | TAC study | | | | ACF study | | | |
|---|---|---|---|---|---|---|---|---|
| | WT | | N2B KO | | WT | | N2B KO | |
| | SHAM | TAC | SHAM | TAC | SHAM | ACF | SHAM | ACF |
| BW (g) | 29 ± 2 | 30 ± 3 | 29 ± 2 | 28 ± 2 | 29 ± 4 | 26 ± 1 | 27 ± 5 | 27 ± 3 |
| LV (mg) | 83.9 ± 8.1 | 118.6 ± 20.9**** | 72.9 ± 5.2 | 114.5 ± 17.3**** | 91.2 ± 4.9 | 102.3 ± 11.1 | 75.8 ± 9.8 | 76.4 ± 6.5### |
| RV (mg) | 27.7 ± 3.7 | 32.1 ± 8.2 | 24.9 ± 3.9 | 28.1 ± 4.2 | 26.0 ± 2.0 | 35.8 ± 3.6** | 23.2 ± 3.8 | 26.4 ± 3.8#### |
| LA (mg) | 4.1 ± 0.7 | 6.1 ± 2.0 | 4.7 ± 2.8 | 7.7 ± 3.2 | 4.0 ± 0.7 | 7.6 ± 1.2* | 5.6 ± 0.6 | 10.6 ± 3.8* |
| RA (mg) | 3.2 ± 0.8 | 4.1 ± 0.9 | 3.8 ± 2.2# | 4.8 ± 1.3 | 3.3 ± 0.6 | 6.4 ± 1.0**** | 4.7 ± 0.4# | 8.7 ± 1.8****## |
| LV/BW (mg/g) | 2.92 ± 0.17 | 4.01 ± 0.53**** | 2.52 ± 0.21 | 4.16 ± 0.68**** | 3.14 ± 0.31 | 3.95 ± 0.31**** | 2.85 ± 0.29 | 2.82 ± 0.23#### |
| RV/BW (mg/g) | 0.96 ± 0.09 | 1.09 ± 0.29 | 0.86 ± 0.15 | 1.02 ± 0.13 | 0.90 ± 0.07 | 1.39 ± 0.12 | 0.87 ± 0.12 | 0.98 ± 0.17 |
| LA/BW (mg/g) | 0.14 ± 0.02 | 0.21 ± 0.06 | 0.20 ± 0.03 | 0.28 ± 0.12 | 0.14 ± 0.02 | 0.29 ± 0.05 | 0.21 ± 0.04 | 0.39 ± 0.10 |
| RA/BW (mg/g) | 0.11 ± 0.02 | 0.14 ± 0.03 | 0.16 ± 0.02## | 0.17 ± 0.04# | 0.11 ± 0.02 | 0.25 ± 0.03 | 0.18 ± 0.03 | 0.32 ± 0.07 |

| | SWIMMING STUDY | | | | Isoproterenol STUDY | | | |
|---|---|---|---|---|---|---|---|---|
| | WT | | N2B KO | | WT | | N2B KO | |
| | SED | SWIM | SED | SWIM | saline | ISO | saline | ISO |
| BW (g) | 26 ± 1 | 25 ± 1 | 27 ± 2 | 26 ± 2 | 28 ± 2 | 28 ± 1 | 28 ± 2 | 28 ± 2 |
| LV (mg) | 76.2 ± 4.3 | 88.8 ± 11.2** | 69.3 ± 6.7 | 72.3 ± 6.3#### | 78.4 ± 5.3 | 96.1 ± 8.4**** | 73.4 ± 6.3 | 77.2 ± 8.0#### |
| RV (mg) | 25.1 ± 1.8 | 27.2 ± 4.0 | 22.3 ± 2.2 | 24.7 ± 3.0 | 26.8 ± 2.2 | 30.4 ± 5.4 | 24.5 ± 3.0 | 26.2 ± 3.7 |
| LA (mg) | 3.0 ± 0.5 | 3.9 ± 0.6* | 5.3 ± 0.6#### | 6.7 ± 1.1 ***#### | 3.1 ± 0.3 | 3.9 ± 0.5 | 5.4 ± 0.7#### | 6.7 ± 1.0***#### |
| RA (mg) | 2.4 ± 0.5 | 3.5 ± 0.8* | 4.6 ± 0.6#### | 5.2 ± 1.1#### | 2.8 ± 0.4 | 3.7 ± 0.5 | 4.6 ± 0.5#### | 4.7 ± 1.2# |
| LV/BW (mg/g) | 2.97 ± 0.14 | 3.52 ± 0.28* | 2.54 ± 0.16## | 2.78 ± 0.16### | 2.84 ± 0.17 | 3.43 ± 0.20**** | 2.58 ± 0.12# | 2.78 ± 0.23#### |
| RV/BW (mg/g) | 0.98 ± 0.06 | 1.08 ± 0.13 | 0.82 ± 0.08## | 0.95 ± 0.07* | 0.97 ± 0.10 | 1.07 ± 0.16 | 0.86 ± 0.06 | 0.94 ± 0.09# |
| LA/BW (mg/g) | 0.12 ± 0.02 | 0.16 ± 0.02 | 0.19 ± 0.02## | 0.26 ± 0.03****#### | 0.11 ± 0.02 | 0.14 ± 0.02 | 0.19 ± 0.02#### | 0.24 ± 0.03 ********#### |
| RA/BW (mg/g) | 0.09 ± 0.02 | 0.14 ± 0.03* | 0.17 ± 0.02## | 0.20 ± 0.03*## | 0.10 ± 0.02 | 0.13 ± 0.02* | 0.16 ± 0.01#### | 0.17 ± 0.03## |

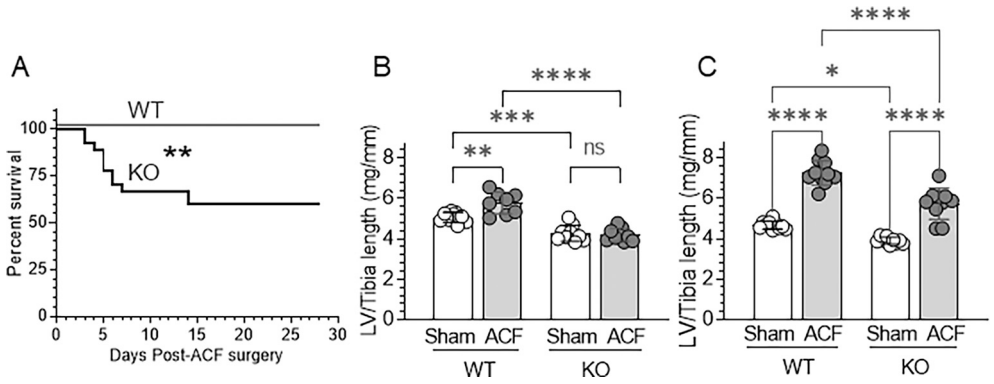


**Fig. 2.** Blunted hypertrophic response to volume-overload in N2B KO mice. A) Survival curve. Curves are significant different ($p = 0.005$). B) LV mass normalized to tibia length after 1-week ACF (B) and 4 weeks (C). Data shown as mean ± SD. ACF significantly increases LV mass in WT mice but has significantly reduced effects in N2B KO mice. Two-way ANOVA in B) reveals a significant effect of ACF on LV mass ($p = 0.02$) and a significant effect of genotype ($p \leq 0.0001$) with KO animals having lower mean values. Two-way ANOVA in C) reveals a significant effect of ACF on LV mass ($p < 0.0001$) and a significant effect of genotype ($p \leq 0.0001$) with KO animals having lower mean values. Results of post-hoc analyses shown on the figure. Additional details of statistical analyses are in Supplemental Table 3. Data shown as mean ± SD. *:$p < 0.05$; **:$p < 0.01$; ***:$p < 0.001$; ****:$p < 0.0001$.

compensate for the increase in wall stress that results from the increase in LV chamber size. The finding that wall thickness does not increase in KO mice indicates that this compensation does not occur, which is likely to contribute to the poor survival of KO mice post ACF surgery (Fig. 2A). Thus, the N2B element is necessary for mediating early volume overload-induced cardiac remodeling observed in WT mice, particularly within the first week. Considering the significant mortality within the first week, this suggests that the failure of N2B KO mice to undergo hypertrophic remodeling is a critical factor contributing to increased mortality during that period.

In addition to the pathological model of chronic volume overload represented by ACF, exercise training serves as a physiologically

relevant approach that increases preload and triggers cardiac hypertrophy [30]. To assess the involvement of the N2B element in a more physiological context of volume-induced cardiac hypertrophy, mice were subjected to a swimming protocol. Following the completion of the swimming study, WT mice exhibited a 14.6 ± 3.5% increase in normalized LV mass (mean ± SD, $n = 9$), while the hypertrophy observed in KO mice was significantly attenuated ($p = 0.0007$) with a value of 8.9 ± 1.5% (mean ± SD, $n = 10$), as shown in Fig. 3. These findings highlight the crucial role of the N2B element in physiological volume-overload induced hypertrophy.

### 3.3. N2B KO attenuates p38 MAPK activation following ACF

RNA-seq was performed on LV of 1-week ACF mice to gain insights into potential signaling pathways behind the attenuated hypertrophy response of N2B KO mice. WT ACF mice had 1332 differentially expressed genes, relative to WT shams (Fig. 4A) and N2B KO ACF mice has 780 differentially expressed genes, relative to N2B KO sham (Fig. 4B). Between sham groups (WT and N2B KO) 14 genes were found to be differentially expressed (Fig. 4C and Supplemental Table 1), and between ACF groups (WT and N2B KO) 106 differentially expressed genes were found (Fig. 4D and Supplemental Table 2). MAP3K20 was amongst the genes that were most significantly different. MAP3K20 is a mitogen activated protein kinase (MAPK) kinase, which mediates the adrenergic response through p38 MAPK activation [31]. mRNA expression of several components of the adrenergic-p38 activating pathway, including EPAC1/2 (Rapgef3 and Rapgef4), p38 MAPK (Mapk11), and MEF2C, were also identified as being differentially regulated in the ACF responses for WT and N2B KO mice (Fig. 4). Western blot analysis revealed that p38 MAPK phosphorylation (Thr180/Tyr182) is increased 1-week post-ACF in WT mice but is unchanged in N2B KO mice, suggesting that activation of p38 MAPK might be involved in the ACF hypertrophy response (Fig. 5A).

p38 MAPK involvement in the cardiac hypertrophy response has been clouded by conflicting results from in vitro data demonstrating a pro-hypertrophy role [32,33] and in vivo data demonstrating an anti-hypertrophy role [34,35]; however, work from Striecher et al. [36] demonstrated that physiologically relevant short-term activation of p38 MAPK mediates cardiac hypertrophy. This suggests that the inability of p38 MAPK to be activated in N2B KO mice in response to ACF reflects a disconnect in upstream signaling pathways and may contribute to the hypertrophy deficit.

In addition to p38 MAPK, common canonical hypertrophy pathways were evaluated by Western Blot analysis. Antibodies against known activating phosphorylation sites for AKT, ERK1/2, and GSK3β failed to support that these pathways are active above baseline levels at 1-week post-ACF in either genotype (Fig. 5B-D). Protein levels of Calcineurin (CaN), another key regulator of cardiac hypertrophy, were similarly unchanged with ACF (Fig. 5E). Calcineurin activity was also assessed directly, as protein levels are not indicative of activity, and this revealed that CaN activity is unaltered 1-week post-ACF in both genotypes (Fig. 5F). These same hypertrophy regulators were assessed under baseline conditions; however, no difference except for a small but statistically significant increase in phosphorylated GSK3β was observed (Supplemental Fig. 5 A-E). Following sham or ACF surgery no differences in phosphorylated GSK3β were observed between any groups (Fig. 5D), suggesting GSK3β may not be a key player in the ACF hypertrophy response.

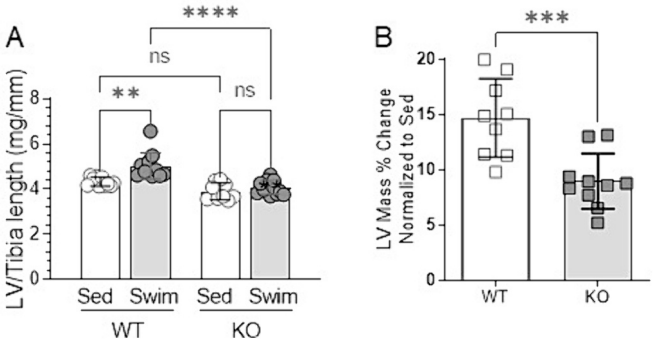


**Fig. 3.** Hypertrophic response to swimming exercise is reduced in N2B KO mice. A) Left ventricular (LV) mass normalized to tibia length. Two-way ANOVA in A) reveals a significant effect of swimming on LV mass ($p = 0.001$) and a significant effect of genotype ($p \leq 0.0001$) with KO animals having lower mean values. Results of post-hoc analyses shown on the fig. B) Percent left ventricle (LV) mass increase in swim study. Additional details of statistical analyses are in Supplemental Table 3. Data shown as mean ± SD. **:$p < 0.01$; ***:$p < 0.001$; ****:$p < 0.0001$.

### 3.4. Expression of titin-binding proteins

To the best of our knowledge, a direct link between the N2B element and p38 MAPK activation has yet to be identified. However, the N2B binding proteins FHL1 and FHL2 have been implicated in the activation of MAPK pathways including ERK1/2 [26,37] and p38 MAPK [22,38,39]. FHL1 protein levels were unchanged between genotypes and in response to volume overload (Fig. 6A). FHL2 protein levels have been demonstrated to be greatly reduced (>90%) in N2B KO mice [19] and we confirmed this finding in both N2B KO sham and ACF samples (Fig. 6B). FHL2 transcript was not significantly changed in N2B KO animals, neither in SHAM nor in ACF samples (Supplemental Fig. 6), suggesting that FHL2 is either regulated post-transcriptionally or protein stability is decreased in the absence of titin's N2B element. This is consistent with previous work on the N2B KO LV, in which FHL2 protein levels were greatly reduced while FHL2 transcript was unchanged [19]. In addition to being linked to the p38 MAPK pathway, FHL2 has been identified as a modifier of the hypertrophic response to adrenergic stimulation [20,21], offering a potential link between the N2B element, activation of p38 MAPK, and adrenergic signaling identified by RNA-Seq.

### 3.5. Isoproterenol-induced Hypertrophy is attenuated in N2B KO Mice

To gain further insight into the role of the N2B element in adrenergic stimulation-induced hypertrophy, we conducted experiments involving the administration of isoproterenol, a nonspecific beta agonist, as a pharmacological model of cardiac hypertrophy. Consistent with previous findings, WT mice exhibited significant left ventricular hypertrophy (20.4 ± 6.8% increase) following isoproterenol treatment (Fig. 7A-B). In contrast, N2B KO mice displayed attenuated hypertrophy (7.6 ± 8.8% increase, Fig. 7A-B). Furthermore, the levels of FHL1 protein were elevated in both WT and N2B KO mice in response to isoproterenol although the FHL1 response in the N2B KO was blunted (Fig. 7C) which could potentially be related to the reduced LV hypertrophy of the N2B KO (see also Discussion). While FHL2 levels were reduced in WT mice following isoproterenol treatment, no further decrease was observed in N2B KO mice (Fig. 7D). These results suggest that the N2B element plays a significant role in the hypertrophic response to adrenergic stimulation, and FHL2 may serve as a critical effector within this pathway.

## 4. Discussion

The heart's ability to perceive and adapt to changes in mechanical load is crucial for maintaining cardiac function during development and in response to hemodynamic stress. Titin, spanning from the *Z*-disc to the M-band in the half sarcomere, is strategically positioned within cardiac myocytes to sense alterations in loading conditions. Hence, titin has been previously proposed as a mechanosensor that translates mechanical load changes into downstream signaling events [3,40,41]. Within the extensible I-band of cardiac titin, there exists a unique

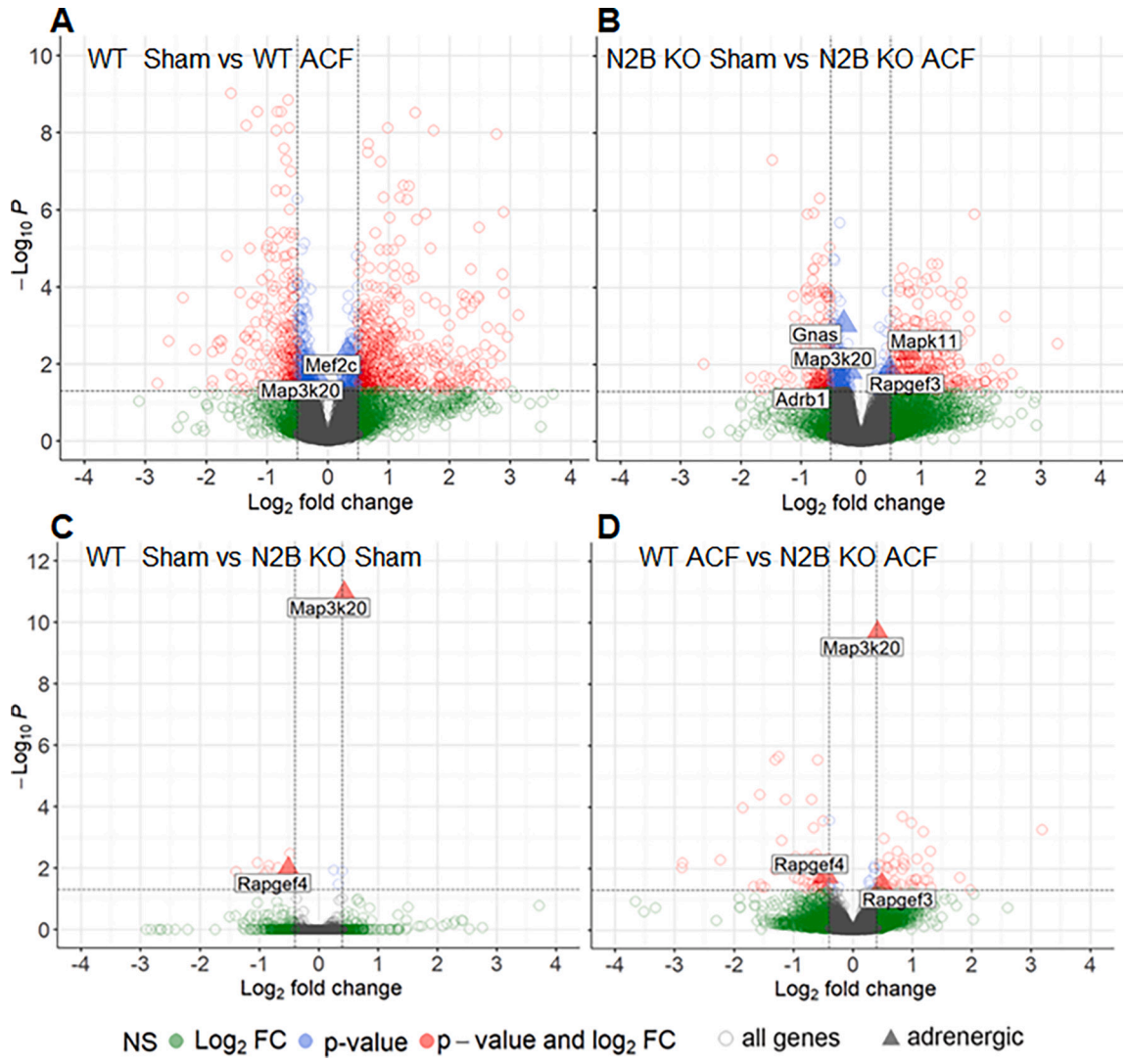


**Fig. 4.** ACF (1 week) RNA-Seq Profile. Volcano plot of RNA-Seq gene expression between WT sham and WT ACF (A); N2B KO sham and N2B KO ACF (B); WT sham and N2B KO sham (C) and WT ACF and N2B KO ACF (D) samples. Significant differentially regulated genes (DEGs) involved in the adrenergic pathway are labeled (triangles). Note: PDE11A and OSBPL6 and HHIPL1 were excluded from the plots in order to improve visibility (their values are given in Supplemental Tables 1 and 2).

cardiac-specific sequence known as the N2B element. This element has been shown to interact with various scaffolding proteins and signaling enzymes, positioning it as a promising candidate for facilitating mechanotransduction [11,26,42]. The findings presented in this study demonstrate that while the N2B element is not essential for hypertrophy induced by afterload, it plays a significant role in initiating the cardiac hypertrophic response to volume overload and exercise.

Earlier studies suggested that the N2B element plays a significant role in initiating the hypertrophic response to pressure overload resulting from transverse aortic constriction (TAC) and proposed that the N2B element mediates hypertrophic signaling through interactions with FHL1 and MAPK [26]. However, our findings challenge the notion that the N2B element is crucial for initiating pressure overload-induced hypertrophy, as N2B KO mice exhibited robust hypertrophy in response to TAC. Therefore, a revision of this model might be required. While the significance of previous research highlights the critical role of the FHL1/MAPK pathway in mediating the hypertrophic response after TAC is evident [26], it appears that the observed interaction at the N2B element is not essential for this process. However, our finding that volume overload-induced hypertrophy is attenuated in the N2B KO mouse (see also below), suggests that volume overload-induced hypertrophy might involve a mechanosensing complex that is N2B element based. Whether it is dependent on FHL1 could be tested in future studies by addressing the effect of volume overload in the FHL1 KO mouse model [26].

In contrast to their robust hypertrophy response to TAC, N2B KO mice demonstrated a dramatic hypertrophy deficit and a high mortality rate following aortocaval fistula (ACF) -induced volume overload. Wall thickening due to hypertrophy serves as an adaptive remodeling mechanism in response to volume overload, aiming to reduce elevated wall stress and preserve cardiac function. The failure of N2B KO mice to adequately remodel in the presence of volume overload likely plays a major role in the observed increased mortality rate. No evidence of left ventricular rupture, or complications at the surgical site was detected, and the exact cause of death in these mice remains to be determined. The timing of the increased mortality emphasizes the importance of the N2B element in sensing the elevated load and initiating the early compensatory remodeling crucial for survival.

The ACF model represents a sudden and extreme form of volume overload, and its closest pathological comparisons may include conditions such as post-traumatic/surgical arterio-venous shunt or mitral regurgitation. However, our findings suggest that the N2B element is not only involved in pathological hypertrophy but also plays a significant

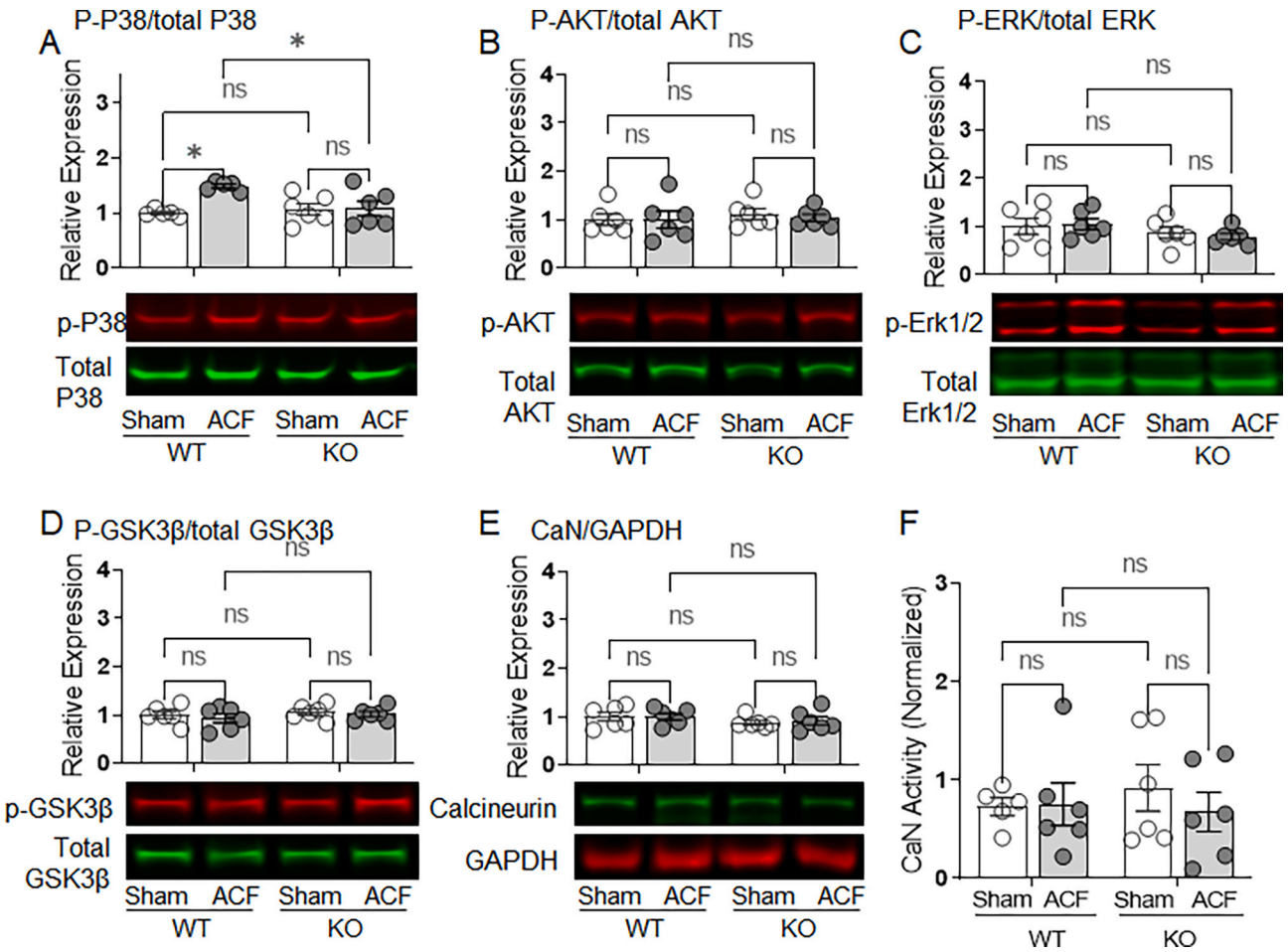


**Fig. 5.** Canonical hypertrophy pathways assayed during volume-overload (1-week ACF). Western Blot analysis of p-P38/total P38 (A), p-AKT/total AKT (B), p-ERK/total ERK (C), p-GSK3β/total GSK3β (D), and calcineurin/GAPDH (E) in WT and N2B KO mice 1-week post sham/ACF surgery. Calcineurin activity assay was performed using LV lysate from 1-week post-surgery samples (F). Results of two-way ANOVA only shows significant results in A: effect of ACF surgery is significant ($p = 0.02$). Results of post-hoc analyses shown on the figure. Data shown as mean ± SD. Details of statistical analyses are in Supplemental Table 3. *:$p < 0.05$.

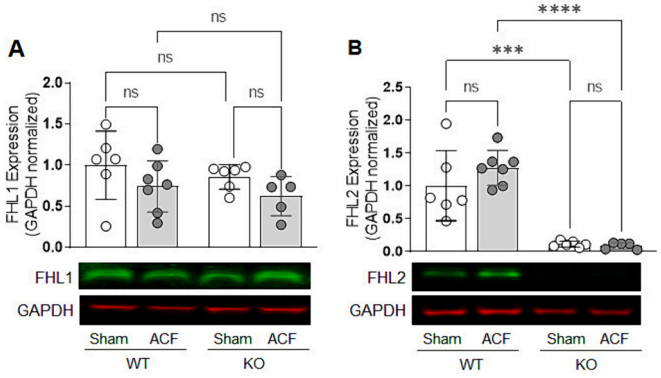


**Fig. 6.** Titin binding protein expression during volume-overload (1-week ACF). Western Blot analysis of titin binding partners FHL1 (A) and FHL2 (B). Data shown as mean ± SD. Two-way ANOVA reveals no significant effect of ACF ($p = 0.06$) and no significant effect of genotype on FHL1 expression. Two-Way ANOVA reveals no significant effect of ACF but a significant genotype effect ($p < 0.0001$) on FHL2 expression with reduced mean values in the KO mice. Results of post-hoc analysis shown on the figures. Details of statistical analyses are in Supplemental Table 3. ***:$p < 0.001$; ****:$p < 0.0001$.

role in physiological hypertrophy that occurs during exercise. Physiological hypertrophy, like its pathological counterpart, is a response of the heart to stress triggered by changes in loading conditions and altered neurohormonal signaling. Endurance swimming, for example, leads to prolonged periods of increased heart rate, stroke volume, and cardiac output, resulting in elevated volume load on the heart. It has been well-documented that endurance swimming promotes cardiac hypertrophy [43,44]. The observed attenuated exercise-induced hypertrophy in N2B KO mice, along with the results from the ACF study, indicates that the N2B element is an important mediator of volume overload-induced hypertrophy under both pathological and physiological conditions.

The reason for the significant role of the N2B element in volume overload-induced hypertrophy compared to pressure overload may be attributed to the conformational changes it undergoes in response to preload versus afterload conditions. Positioned within the I-band region of titin, the N2B element contributes to the extensibility of titin, extending extensively towards the upper limit of the physiological sarcomere length range [9,45]. When preload increases, the end-diastolic sarcomere length is abruptly increased, leading to greater extension of the N2B element during diastole. This contrasts with increased afterload where such abrupt sarcomere length increase will be absent. The higher extension of the N2B element in the case of volume overload might expose or obstruct binding sites within its domain for various interacting proteins and signaling cascades, potentially acting as a sophisticated mechanical sensor. Notably, multiple proteins such as FHL1, FHL2, and alpha B-crystalline (αBC) have been demonstrated to

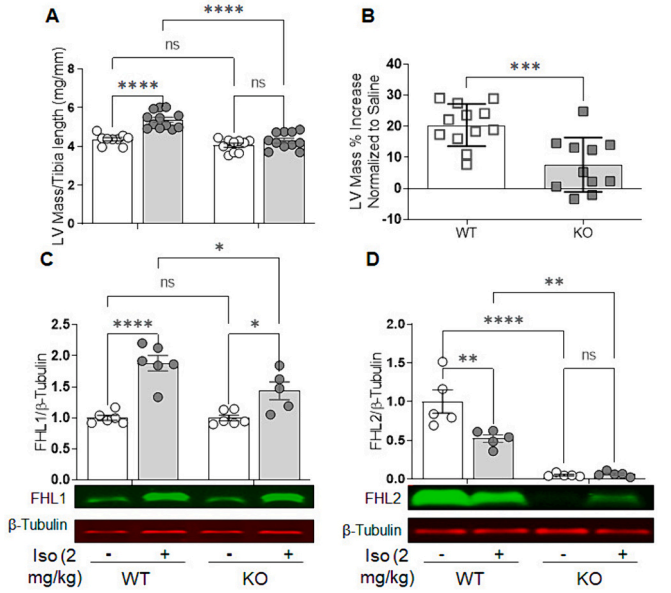


**Fig. 7.** Isoproterenol-induced hypertrophy is attenuated in N2B KO mice. A) LV mass normalized to tibia length following 5-day isoproterenol treatment (2 mg/kg/day). Two-way ANOVA reveals a significant effect of Iso on LV mass ($p < 0.0001$) and a significant effect of genotype ($p < 0.0001$) with KO animals having lower mean values. Results of post-hoc analyses shown on the fig. B) % increase in LV mass normalized to saline control reveals a reduced Iso effect in KO mice. Western blot analysis of FHL1 (C) and FHL2 (D) protein levels following isoproterenol. Two-way ANOVA reveals a significant Iso effect on FHL1 expression ($p < 0.0001$) and a significant effect of genotype ($p = 0.03$) with lower mean values in KO mice. Two-way ANOVA reveals a significant Iso effect on FHL2 expression ($p = 0.01$) and a significant effect of genotype ($p < 0.0001$) with lower mean values in KO mice. Results of posthoc analyses are shown on the figures. Data shown as mean ± SD. Details of statistical analyses are in Supplemental Table 3. *:$p < 0.05$; **:$p < 0.01$; ***:$p < 0.001$; ****:$p < 0.0001$.

bind to the N2B element [11,26,42].

Despite the unchanged levels of FHL1 and αBC between WT and N2B KO mice at baseline (Supplemental Fig. 5F), a notable reduction is observed in FHL2 levels. FHL2 is well-known for its role as a repressor of cardiac hypertrophy [20,21], and yet, the N2B KO mice exhibit attenuated volume-overload hypertrophy, despite the significantly reduced FHL2 levels. The reported function of FHL2 (suppressing hypertrophy) leads to an expected increase in hypertrophy in the N2B KO where FHL2 is >90% reduced, but, in contrast, hypertrophy was observed to be attenuated in volume overload N2B KO mice. Previous studies, such as Okamoto et al. [22], have shown co-localization of FHL2 with ROCK2 in the perinuclear region, and a point mutation in FHL2 that disrupts its binding to the N2B element has been associated with familial dilated cardiomyopathy [46]. The disruption of FHL2 localization to the sarcomere could enhance its ability to block p38 MAPK activation. According to a proposed mechanism [47], increased strain on titin leads to greater binding of FHL2, resulting in sequestration of FHL2 at the sarcomere. FHL2 knockdown studies have demonstrated p38 MAPK activation in non-cardiac tissues lacking sarcomeres and N2B binding sites [38,39,48]. Therefore, in conditions of heightened titin strain, such as during volume overload, increased binding of FHL2 at the sarcomere may enhance p38 MAPK activation and the hypertrophy response by relieving FHL2 inhibition. While this represents a possible mechanism, further investigations are required to fully elucidate the N2B-FHL2-p38 MAPK mechanosensing signalosome.

### 4.1. Study limitations

The N2B KO model has a baseline phenotype that includes diastolic dysfunction and mild LV weight deficiency [19]. It cannot be excluded that some of these baseline changes impact the outcome to either pressure or volume overload. However, if a N2B-based mechanosensory system that converts pressure overload to a hypertrophy signal were to exist, it would be surprising that its absence would be countered by some aspect of the N2B KO's baseline phenotype. Additionally, our findings only apply to the time points that were studied, i.e., the attenuated hypertrophy response to volume overload in the N2B KO was present 1- and 4-weeks post ACF surgery, but it is possible that it does not persistent far beyond 4 weeks. Our conclusion that the N2B element plays a role in volume-overload adaptation of the heart only applies to the early volume-overload response.

In summary, the intricate nature of molecular networks and their interaction with mechanical stimuli has posed challenges in identifying and characterizing mechanotransduction pathways. Nevertheless, progress has been made in unraveling the mechanisms underlying the conversion of mechanical signals into physiological responses. The findings presented in this study shed light on the significant role played by the N2B element in mediating cardiac remodeling in response to increased preload, both in pathological and physiological contexts. Conversely, the N2B element appears not to be required for hypertrophy induced by afterload. While the precise mechanism of N2B mechanosensing remains to be fully understood, our study represents a significant advancement in comprehending the importance of titin in mechanotransduction processes.

## CRediT authorship contribution statement

**Joshua Strom:** Writing – review & editing, Data curation, Formal analysis, Writing – original draft. **Mathew Bull:** Writing – original draft, Data curation. **Jochen Gohlke:** Data curation, Formal analysis, Writing – review & editing. **Chandra Saripalli:** Conceptualization. **Mei Methawasin:** Formal analysis, Writing – review & editing. **Michael Gotthardt:** Conceptualization, Writing – review & editing. **Henk Granzier:** Conceptualization, Project administration, Supervision, Writing – original draft.

## Declaration of competing interest

The authors have declared that no conflict of interest exists.

## Acknowledgments

This research was supported by National Institutes of Health R35HL144998 (H.G.). We thank the UA Phenotyping Core (UAPC) (RRID:SCR_023879) for their assistance with the echocardiography studies.

## Appendix A. Supplementary data

Supplementary data to this article can be found online at https://doi.org/10.1016/j.yjmcc.2024.04.006.

## References

[1] B.C. Bernardo, et al., Molecular distinction between physiological and pathological cardiac hypertrophy: experimental findings and therapeutic strategies, Pharmacol. Ther. 128 (1) (2010) 191–227.
[2] M. Vidal, et al., beta-adrenergic receptor stimulation causes cardiac hypertrophy via a Gbetagamma/Erk-dependent pathway, Cardiovasc. Res. 96 (2) (2012) 255–264.
[3] R.C. Lyon, et al., Mechanotransduction in cardiac hypertrophy and failure, Circ. Res. 116 (8) (2015) 1462–1476.

[4] B.R. Anderson, H.L. Granzier, Titin-based tension in the cardiac sarcomere: molecular origin and physiological adaptations, Prog. Biophys. Mol. Biol. 110 (2–3) (2012) 204–217.
[5] M. Hoshijima, Mechanical stress-strain sensors embedded in cardiac cytoskeleton: Z disk, titin, and associated structures, Am. J. Physiol. Heart Circ. Physiol. 290 (4) (2006) H1313–H1325.
[6] H. Granzier, et al., Titin: physiological function and role in cardiomyopathy and failure, Heart Fail. Rev. 10 (3) (2005) 211–223.
[7] M. Gautel, E. Lehtonen, F. Pietruschka, Assembly of the cardiac I-band region of titin/connectin: expression of the cardiac-specific regions and their structural relation to the elastic segments, J. Muscle Res. Cell Motil. 17 (4) (1996) 449–461.
[8] M. Rief, et al., Single molecule force spectroscopy of spectrin repeats: low unfolding forces in helix bundles, J. Mol. Biol. 286 (2) (1999) 553–561.
[9] K. Trombitas, et al., Molecular dissection of N2B cardiac titin's extensibility, Biophys. J. 77 (6) (1999) 3189–3196.
[10] M. Helmes, et al., Mechanically driven contour-length adjustment in rat cardiac titin's unique N2B sequence: titin is an adjustable spring, Circ. Res. 84 (11) (1999) 1339–1352.
[11] S. Lange, et al., Subcellular targeting of metabolic enzymes to titin in heart muscle may be mediated by DRAL/FHL-2, J. Cell Sci. 115 (Pt 24) (2002) 4925–4936.
[12] R. Yamasaki, et al., Protein kinase a phosphorylates titin's cardiac-specific N2B domain and reduces passive tension in rat cardiac myocytes, Circ. Res. 90 (11) (2002) 1181–1188.
[13] M. Kruger, et al., Protein kinase G modulates human myocardial passive stiffness by phosphorylation of the titin springs, Circ. Res. 104 (1) (2009) 87–94.
[14] C.G. Hidalgo, et al., The multifunctional ca(2+)/calmodulin-dependent protein kinase II delta (CaMKIIdelta) phosphorylates cardiac titin's spring elements, J. Mol. Cell. Cardiol. 54 (2013) 90–97.
[15] N. Hamdani, et al., Crucial role for Ca2(+)/calmodulin-dependent protein kinase-II in regulating diastolic stress of normal and failing hearts via titin phosphorylation, Circ. Res. 112 (4) (2013) 664–674.
[16] K.R. Hutchinson, et al., Increased myocardial stiffness due to cardiac titin isoform switching in a mouse model of volume overload limits eccentric remodeling, J. Mol. Cell. Cardiol. 79 (2015) 104–114.
[17] J. Perkin, et al., Phosphorylating Titin's cardiac N2B element by ERK2 or CaMKIIdelta lowers the single molecule and cardiac muscle force, Biophys. J. 109 (12) (2015) 2592–2601.
[18] M.K. Miller, et al., The sensitive giant: the role of titin-based stretch sensing complexes in the heart, Trends Cell Biol. 14 (3) (2004) 119–126.
[19] M.H. Radke, et al., Targeted deletion of titin N2B region leads to diastolic dysfunction and cardiac atrophy, Proc. Natl. Acad. Sci. USA 104 (9) (2007) 3444–3449.
[20] Y. Kong, et al., Cardiac-specific LIM protein FHL2 modifies the hypertrophic response to -adrenergic stimulation, Circulation 103 (22) (2001) 2731–2738.
[21] B. Hojayev, et al., FHL2 binds calcineurin and represses pathological cardiac growth, Mol. Cell. Biol. 32 (19) (2012) 4025–4034.
[22] R. Okamoto, et al., FHL2 prevents cardiac hypertrophy in mice with cardiac-specific deletion of ROCK2, FASEB J. 27 (4) (2013) 1439–1449.
[23] M.H. Radke, et al., Targeted deletion of titin N2B region leads to diastolic dysfunction and cardiac atrophy, Proc. Natl. Acad. Sci. USA 104 (9) (2007) 3444–3449.
[24] P. Hu, et al., Minimally invasive aortic banding in mice: effects of altered cardiomyocyte insulin signaling during pressure overload, Am. J. Physiol. Heart Circ. Physiol. 285 (3) (2003) H1261–H1269.
[25] M.L. Bang, et al., The complete gene sequence of titin, expression of an unusual approximately 700-kDa titin isoform, and its interaction with obscurin identify a novel Z-line to I-band linking system, Circ. Res. 89 (11) (2001) 1065–1072.
[26] F. Sheikh, et al., An FHL1-containing complex within the cardiomyocyte sarcomere mediates hypertrophic biomechanical stress responses in mice, J. Clin. Invest. 118 (12) (2008) 3870–3880.
[27] K.T. Weber, et al., Fibrillar collagen and remodeling of dilated canine left ventricle, Circulation 82 (4) (1990) 1387–1401.
[28] K.R. Hutchinson, et al., Temporal pattern of left ventricular structural and functional remodeling following reversal of volume overload heart failure, J. Appl. Physiol. (1985) 111 (6) (2011) 1778–1788.
[29] T.D. Ryan, et al., Left ventricular eccentric remodeling and matrix loss are mediated by bradykinin and precede cardiomyocyte elongation in rats with volume overload, J. Am. Coll. Cardiol. 49 (7) (2007) 811–821.
[30] M. Nakamura, J. Sadoshima, Mechanisms of physiological and pathological cardiac hypertrophy, Nat. Rev. Cardiol. 15 (7) (2018) 387–407.
[31] L. Cariolato, S. Cavin, D. Diviani, A-kinase anchoring protein (AKAP)-Lbc anchors a PKN-based signaling complex involved in α1-adrenergic receptor-induced p38 activation, J. Biol. Chem. 286 (10) (2011) 7925–7937.
[32] Y. Wang, et al., Cardiac muscle cell hypertrophy and apoptosis induced by distinct members of the p38 mitogen-activated protein kinase family, J. Biol. Chem. 273 (4) (1998) 2161–2168.
[33] Q. Liang, J.D. Molkentin, Redefining the roles of p38 and JNK signaling in cardiac hypertrophy: dichotomy between cultured myocytes and animal models, J. Mol. Cell. Cardiol. 35 (12) (2003) 1385–1394.
[34] J.J. Martindale, et al., Overexpression of mitogen-activated protein kinase kinase 6 in the heart improves functional recovery from ischemia in vitro and protects against myocardial infarction in vivo, J. Biol. Chem. 280 (1) (2005) 669–676.
[35] P. Liao, et al., The in vivo role of p38 MAP kinases in cardiac remodeling and restrictive cardiomyopathy, Proc. Natl. Acad. Sci. USA 98 (21) (2001) 12283–12288.
[36] J.M. Streicher, et al., MAPK-activated protein kinase-2 in cardiac hypertrophy and cyclooxygenase-2 regulation in heart, Circ. Res. 106 (8) (2010) 1434–1443.
[37] N.H. Purcell, et al., Extracellular signal-regulated kinase 2 interacts with and is negatively regulated by the LIM-only protein FHL2 in cardiomyocytes, Mol. Cell. Biol. 24 (3) (2004) 1081–1095.
[38] C.H. Wong, et al., The LIM-only protein FHL2 regulates interleukin-6 expression through p38 MAPK mediated NF-κB pathway in muscle cells, Cytokine 59 (2) (2012) 286–293.
[39] V. Wixler, et al., FHL2 regulates the resolution of tissue damage in chronic inflammatory arthritis, Ann. Rheum. Dis. 74 (12) (2015) 2216–2223.
[40] H.L. Granzier, S. Labeit, The giant protein titin: a major player in myocardial mechanics, signaling, and disease, Circ. Res. 94 (3) (2004) 284–295.
[41] W.A. Linke, Sense and stretchability: the role of titin and titin-associated proteins in myocardial stress-sensing and mechanical dysfunction, Cardiovasc. Res. 77 (4) (2008) 637–648.
[42] Y. Zhu, et al., Single molecule force spectroscopy of the cardiac titin N2B element: effects of the molecular chaperone alphaB-crystallin with disease-causing mutations, J. Biol. Chem. 284 (20) (2009) 13914–13923.
[43] R.B. Madeira, et al., Effects of chronic exercise training on left ventricular dimensions and function in young athletes, Rev. Port. Cardiol. 27 (7–8) (2008) 909–922.
[44] C. Mihl, W.R. Dassen, H. Kuipers, Cardiac remodelling: concentric versus eccentric hypertrophy in strength and endurance athletes, Neth. Hear. J. 16 (4) (2008) 129–133.
[45] W.A. Linke, et al., I-band titin in cardiac muscle is a three-element molecular spring and is critical for maintaining thin filament structure, J. Cell Biol. 146 (3) (1999) 631–644.
[46] T. Arimura, et al., Structural analysis of four and half LIM protein-2 in dilated cardiomyopathy, Biochem. Biophys. Res. Commun. 357 (1) (2007) 162–167.
[47] M.H. Radke, et al., Deleting full length titin versus the titin M-band region leads to differential Mechanosignaling and cardiac phenotypes, Circulation 139 (15) (2019) 1813–1827.
[48] C.Y. Chen, et al., Deletion of the FHL2 gene attenuates intima-media thickening in a partially ligated carotid artery ligated mouse model, J. Cell. Mol. Med. 24 (1) (2020) 160–173.